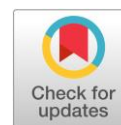# Mechanochemical recrystallization: forgotten basics and new possibilities

Farit Kh. Urakaev [ab] * (ID), Natalya V. Khan [b] (ID), Almagul I. Niyazbayeva [b] (ID), Dinar N. Zharlykasimova [b], Mukhambetkali M. Burkitbayev [b] (ID)

a: Sobolev Institute of Geology and Mineralogy, SB RAS, Novosibirsk 630090, Russia
b: Faculty of Chemistry, Al-Farabi Kazakh National University, Almaty 050040, Kazakhstan
* Corresponding author: urakaev@igm.nsc.ru

This paper belongs to a Regular Issue.

Abstract

The task of this article is to update, develop and introduce into scientific practice the method of "mechanochemical recrystallization" in solid-phase systems with small additives of the liquid phase of the solvent and solid-phase precursors to stabilize the formed nanoparticles. The essence of this method is shown using the example of mechanical activation of the $S–AgNO_3–NH_4X$ system, where X = Cl, Br, I, with the addition of dimethyl sulfoxide (DMSO), and the resulting mechanochemical synthesis of sulfur-containing nanocomposites S/AgX with the controlled content of sulfur nanoparticles (nanosulfur). The predetermined content of nanosulfur in nanocomposites is ensured by a continuous process of dissolution-crystallization (recrystallization) of starting sulfur in the DMSO medium in a mechanochemical reactor. The proposed technical solution made it possible to obtain S/AgX nanocomposites by a single mechanical treatment of powder precursors – $AgNO_3$, NH_4X, NH_4NO_3 (diluent), commercial sulfur and DMSO in planetary ball mills with various milling tools. The method also includes washing the water-soluble components of mechanosynthesis.

Key findings

● A method for synthesis of nanocomposites based on silver halides and sulfur with controlled sulfur content in the DMSO medium is proposed.

● The synthesis is carried out by mechanical activation of powder precursors – sulfur, silver nitrate, ammonium halides and nitrate.

● Nanocomposite formation occurs as a result of reaction process of dissolution-crystallization (recrystallization) of precursors in the DMSO medium.

1. Introduction

The literature describes many examples of mechanochemical transformations that occur upon the addition of small amounts of liquid, and even introduces a special term, Liquid Assisted Grinding (LAG) [1–6]. Typically, the liquid provides the very possibility of the transformation, or affects its rate, or the composition of the products. It is more difficult to find examples where the addition of a liquid was used to control the particle size and composition of the mechanosynthesis product. At the same time, the mechanisms of the influence of liquid on mechanochemical transformations remain debatable, and in many works they are not discussed at all [7–10].

The topic of the article is not related to the well-known phenomenon of "recrystallization" in the process of mechanical activation of solid-phase systems [7–18]. Here it focuses on the possibility of obtaining nanoparticles and nanocomposites by reactive recrystallization of the initial solid precursors from a solution during their processing in a planetary ball mill with the addition of small amounts of liquid DMSO – the precursor solvent [19].

For example, the following ways and results of the implementation of this area of research are known:

– the method of mechanical activation of zinc oxide (ZnO) during its wet grinding with an increase in the solubility of ZnO to a certain level, subsequent

recrystallization and the formation of defects in ZnO crystallites [20];

– the method for the preparation of nanoparticles of calcium carbonate ($CaCO_3$) by high-energy grinding in sodium hypochlorite solutions of waste shells of molluscs *Tapes japonica* with the formation of different phases $CaCO_3$ is associated with mechanical activation of aragonite and dissolution-recrystallization of calcite [21, 22];

– the mechanochemical method for the preparation of nanoparticles of mordenite ($18SiO_2{:}12NaOH{:}780H_2O$) from zeolites, following a strategy of recrystallization with recovery after recrystallization of the crushed sample in a solution of hydrothermal basic silicate of high crystallinity of nano-mordenite with a decrease in the content of phase impurities [23];

– a mechanochemical approach is known for obtaining new solid forms of raloxifene hydrochloride (RHC), which is a benzothiophene derivative with low bioavailability for the treatment of osteoporosis due to its poor solubility in water, based both on its individual grinding and grinding with the addition of liquids [24];

– the effects of adding solvents and grinding times on the formation of a ternary salt were systematically studied, and the formation of a nylon 524T ternary salt under solvent-assisted grinding was found to follow a mechanically driven dissolution-recrystallization mechanism [25];

– the authors of this article described the mechanism of crystalline hydrate mechanosynthesis of nanosulfur [26] and copper sulfide nanocrystals [27, 28] from such precursors as copper acetate, sodium sulfide crystalline hydrate, citric acid, and sodium thiosulfate pentahydrate using wear-resistant milling tools.

The present work is concerned with mechanochemical synthesis, in particular, with the preparation of sulfur-containing nanocomposites of silver halides S/AgX, where X = Cl, Br, I [29, 30] with a controlled content of sulfur. The objective of the article is a systematic study into the method of "mechanochemical recrystallization" in the $AgNO_3$–NH_4X–S solid-phase system with small additions of the solvent phase – DMSO, widely used to dissolve the components of this system [19]. In this case, the controlled content of sulfur in S/AgX and the stabilization of the size of the resulting nanoparticles depend on the initial weight of powdered sulfur and the significant additions to this system of a water-soluble powder diluent – an inert additive or a by-product of the reaction [31], respectively.

The closest in technical essence to the proposed method of "mechanochemical recrystallization" are the solution methods for obtaining nanosulfur [32, 33] and sulfur-containing nanocomposites S / AgX [29, 30, 34] using DMSO. The disadvantage of this method is the impossibility of S / AgX synthesis with a controlled sulfur content. The predetermined content of nanosulfur in nanocomposites is ensured by the process of dissolution-crystallization (recrystallization) of starting sulfur in a universal aprotic solvent DMSO [19] in a mechanochemical reactor [35].

2. Experimental

2.1. Materials and methods

DMSO, $(CH_3)_2SO$, was purchased from Dimethylsulfoxid BioChemica, ≥99.5%, AppliChem GmbH, Darmstadt, Germany. Silver and ammonium nitrates ($AgNO_3$, NH_4NO_3), ammonia halides (NH_4Cl, NH_4Br, NH_4I) and sulfur (S) were purchased from Sigma Aldrich, Germany. For washing, water purified by the purification system Smart2Pure (Thermo Scientific, USA) was used.

The prepared samples were characterized by different techniques. Phase composition of the powders was analyzed by X-ray diffraction (XRD) with a Rigaku MiniFlex 600 X-ray diffractometer using copper radiation (λ = 0.15405 nm). For processing of X-ray diffraction patterns, the ICCD-PDF2 release 2016 database was used.
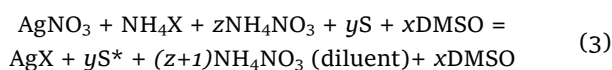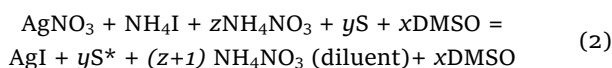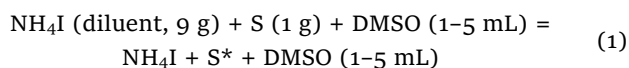
Raman spectra of the samples were recorded on a Solver Spectrum (NT MDT Instruments, Russia) spectrometer using an 1800/500 diffraction grating, which provides a spectral resolution of 1 cm^{-1}. The Raman spectra were excited by a He-Ne laser with a wavelength of 633 nm and processed with help of Origin Lab program.

Size, morphology and elemental composition of the samples were studied by a scanning electron microscope (SEM) Quanta 200i 3D (FEI, Netherlands) equipped by the energy dispersive X-ray analysis (EDAX) sensor. For the analysis, a mixture of 1 g of a sample and 40 ml of water was treated in an ultrasonic bath for 30 minutes. The sample of the resulting suspension was applied to a silicon microscope substrate.

The images of the sulfur nanoparticles (nanosulfur) were produced with a JEOL JEM-1400 transmission electron microscope (TEM; JEOL; Japan) with 80 kV accelerating voltage. The shape and sizes of the nanosulfur were determined by TEM directly at the microscope location by dissolving-washing the mechanosynthesis product with water. The resulting sulfur slurry-colloid was immediately pipetted onto a collodion-coated copper grid for TEM, and nanosulfur images were acquired as soon as possible.

2.2. Mechanochemical preparation

The milling process was realized in the planetary ball mills Pulverisette 6 and 5 (Fritsch, Germany) in a tungsten carbide milling chamber with a volume of 250 mL (1-drum Pulverisette 6) and stainless steel milling chambers with a volume of 1 L (4-drum Pulverisette 5). The milling was performed in air, using tungsten carbide or stainless steel milling balls with a diameter of 10 mm, ball (600 g)-to-powder (10 g) ratio of 60, rotation speed of the planet carrier of 350 min^{-1}, and a milling time of up to 30 minutes. Synthesis of nanosulfur and nanocomposites yS*/AgX, where X = Cl, Br, or I, by "mechanochemical recrystallization" was carried out according to the reactions (S – commercial sulfur; S* – sulfur recrystallized from DMSO):

$$NH_4I \text{ (diluent, 9 g)} + S \text{ (1 g)} + DMSO \text{ (1–5 mL)} =$$
$$NH_4I + S^* + DMSO \text{ (1–5 mL)} \tag{1}$$

$$AgNO_3 + NH_4I + zNH_4NO_3 + yS + xDMSO =$$
$$AgI + yS^* + (z+1) \, NH_4NO_3 \text{ (diluent)} + xDMSO \tag{2}$$

$$AgNO_3 + NH_4X + zNH_4NO_3 + yS + xDMSO =$$
$$AgX + yS^* + (z+1)NH_4NO_3 \text{ (diluent)} + xDMSO \tag{3}$$

using Pulverisette 6 for reaction (1), (2), and Pulverisette 5 for (3) with yS^* content 50 wt.% in S^*/AgX.

Advantages of the reactions chosen for the study include: solubility of precursors in DMSO; the absence of water (for example, there are no crystalline hydrates) both in the initial precursors and in the products, except for their slight moistening due to the hygroscopicity of DMSO [36–38]; ease, simplicity and high speed of implementation.

The essence of this approach is shown in Scheme 1 (see also Figures S1–S5 in the Supplementary materials). It gives examples of the production of nanosulfur in a Pulverisette 6 mill (Scheme 1a, Figure S1a), and nanocomposites S^* / AgI (Scheme 1b, Figures S3a, b) and S^*/AgX (Scheme 1b, c) by realizing reactions (2) and (3) in the Pulverisette 6 and 5 mills. The addition of the universal solvent, DMSO, and neutral diluents (NH_4I and NH_4NO_3) makes it possible to stabilize the size of the formed sulfur and silver halide nanoparticles in the DMSO medium.

3. Results and Discussion

Essentially, we are studying three processes in DMSO: (i) preparation of nanosulfur (S^*) by mechanochemical recrystallization of the initial sulfur; (ii) mechanosynthesis of nanocomposites based on it with an emphasis on obtaining S^*/AgI; and (iii) the effect of mechanical activation conditions on the synthesis of S^*/AgX nanocomposites.

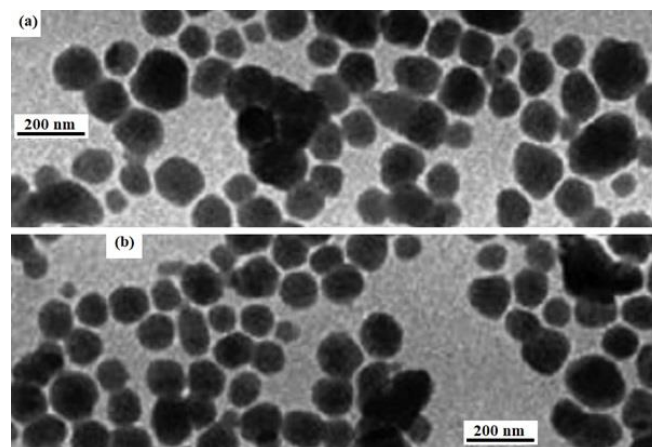### 3.1. Recrystallization of sulfur in DMSO

First, according to reaction (1) and/or Scheme 1a, we carried out the process of mechanochemical recrystallization in DMSO of sulfur with an inert diluent NH4I to prove the transition of sulfur to a nanoscale state. The TEM image of

sulfur particles are shown in Figure 1, and their sizes are in the range of 20–160 nm (average size is about 100 nm) and weakly depend on the amount of added DMSO.

3.1.1. XRD, Raman spectroscopy and SEM-EDAX data

Figure S1a shows that the XRD peaks of the sulfur sample obtained by washing and drying the product of mechanical activation of the system sulfur (1 g) – ammonium iodide (9 g) – DMSO (2 ml) completely correspond to its standard in the ICCD-PDF2 database, PDF Card No. 01-083-2283, in the orthorhombic structure (α–S_8). The XRD software allowed to determine the size of coherent scattering blocks (crystallite size, $D \approx 70$ nm) and lattice microdistortions ($\varepsilon \approx 0.2\%$), see Figure S1b and [39–41].

The review article [42] shows that the α–S_8 vibrational modes at 153 cm^{-1} and 220 cm^{-1} represent, respectively, asymmetric and symmetric bending of the S–S bond. The peak at 473 cm^{-1} is associated with S–S stretching in the S_8 ring. A broad feature at $\approx$440 cm^{-1} is present in all solid sulfur allotropes, and corresponds to S–S stretching modes. A small but distinct peak at 248 cm^{-1} characterizes intramolecular α–S_8 vibrations. External α–S_8 vibrations in the low frequency range are due to a peak at 88 cm^{-1}. These data are almost identical to the Raman spectroscopy of our sulfur sample shown in Figure 2.

Figure 1 TEM images of aqueous suspension in the experiment on "mechanochemical recrystallization" of sulfur (weight 1 g), diluent ammonium iodide (NH4I; 9 g) in the Pulverisette 6 mill with the addition of DMSO (a – 1 mL; b – 5 mL) after dissolution and washing of the diluent and DMSO with water.
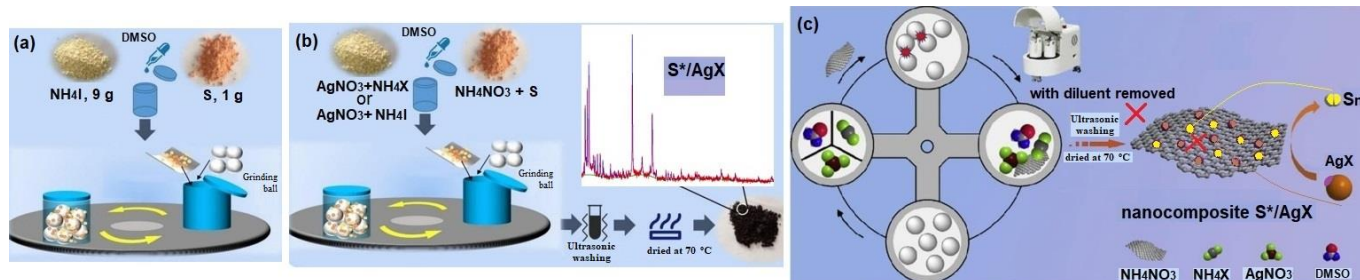
Scheme 1 Schematic representation of the target product synthesis in reactions (1)–(3) by mechanochemical recrystallization in DMSO using planetary mills. Pulverisette 6: nanosulfur with the choice of ammonium iodide as a diluent (a). Pulverisette 6 and Pulverisette 5: S*/AgX or S*/AgI nanocomposites when the by product of reactions (2) and (3), ammonium nitrate is chosen as a diluent (b). Pulverisette 5: preparation of S*/AgX nanocomposites with ultrasonic washing of water-soluble products of mechanosynthesis with water and drying of the target product (c).

According to the SEM images, for example, the sulfur sample on the tab of Figures S2, obtained by washing and drying the product of mechanical activation of the system sulfur (1 g) – ammonium iodide (9 g) – DMSO (3 ml), in the enlarged scale is heterogeneous in size and shape of the particles. We can see the presence of both large and small fractions of spherical, flat and other differently shaped particles, mostly, in the form of submicron agglomerates. The presence of a thin layer on top of large particles is also noticeable. The elemental and 100% content of sulfur composition of the sample on the tab is as expected, since the device could not determine the content of other minor impurities due to technical capabilities.

3.2. Nanocomposites S*/AgI in Pulverisette 6 mill

Similarly, according to reaction (2) and/or Scheme 1b, from precursor powders $AgNO_3$ ($\approx$1.7 g), NH_4I ($\approx$1.5 g), NH_4NO_3 (diluent, $\approx$4.5 g), commercial sulfur ($\approx$2.3 g) and DMSO (1÷5 mL) AgI/S* nanocomposites were obtained in the Pulverisette 6 mill. Samples of AgI/S* (after 3-fold washing of the water-soluble mechanosynthesis components with water using a centrifuge and drying of the resulting target product for 24 hours at 70 °C) were studied by XRD, Raman and SEM-EDAX methods.

Let us comment on the XRD data shown in Figure S3 for the AgI/S* nanocomposites. First, in Figure S3a, the green pointers indicate the AgI lines, which refer to the stable hexagonal phase β–AgI and the metastable cubic phase γ–AgI. Figure S3a is dominated by β–AgI lines, and Figure S3b is dominated by γ–AgI lines. The main sulfur lines, indicated by yellow pointers in Figure S3a, refer to the most stable orthorhombic sulfur phase (S_8), as in Figure S3b.

The results of the processing of XRD data using the Williamson-Hall construction program [39–41] is shown in Figure S4. The data of the Figures S4 (a–d) make it possible to find the values in crystallite sizes D along the indicated segments of the y-axis, and microdistortions of the lattices ε from the tangent of the slope angle of the straight line. The calculated mean values of D = 23 nm show the existence of nanosized blocks of coherent scattering of sulfur and silver iodide particles, and, in terms of ε = 0.22%, also the presence of their defective structure due to mechanical action on crystallites.

The phase composition and component ratio of the AgI/S* nanocomposites was also confirmed by Raman spectroscopy, as shown in Figure S5. It can be seen that there is no significant difference in the spectra of samples 1 (a) and 2 (b). According to the analysis, the sample is represented by silver iodide lines [43]: a peak with a small shoulder at a wave number of $\approx$106 cm^{-1}; a clear peak at 83 cm^{-1} is due to the superposition of the lines of silver iodide at $\approx$74 cm^{-1} and sulfur at 88 cm^{-1} (Figure 2). Other wave numbers, equal to 154, 219, and 473 cm^{-1}, correspond to sulfur in the S_8 modification. An insignificant but noticeable peak at $\approx$246 cm^{-1} indicates intramolecular S_8

vibrations, and a peak at $\approx$437 cm^{-1} can be attributed to both intermolecular S_8 vibrations and the beginning of the S_8 polymerization process [42].

The morphology and particle size were measured by SEM (Figures 3, 4a). The clear SEM image in Figure 3 shows that the AgI/S* composite particles differ in shapes and sizes. A more detailed and enlarged examination of this image can establish that there are agglomerates of smaller particles and, moreover, nanosulfur sediments are found on their surface. The elemental composition of AgI/S* were measured by SEM equipped with an EDAX attachment (Figure 4b, c) from which it can be seen that both the sulfur atomic content and the intensity of the sulfur line are close to those for Ag and I. Similar SEM images are also available for AgCl/S* and AgBr/S*.
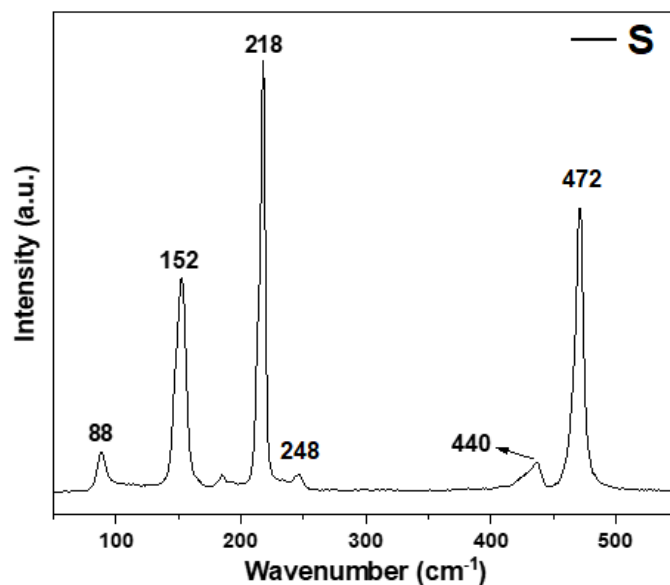
Figure 2 Raman spectroscopy of the sulfur sample obtained by washing and drying the product of mechanical activation according to reaction (1) and/or Scheme 1a with the addition of 2 ml of DMSO (the numbers indicate the correspondence to the data of [42]).
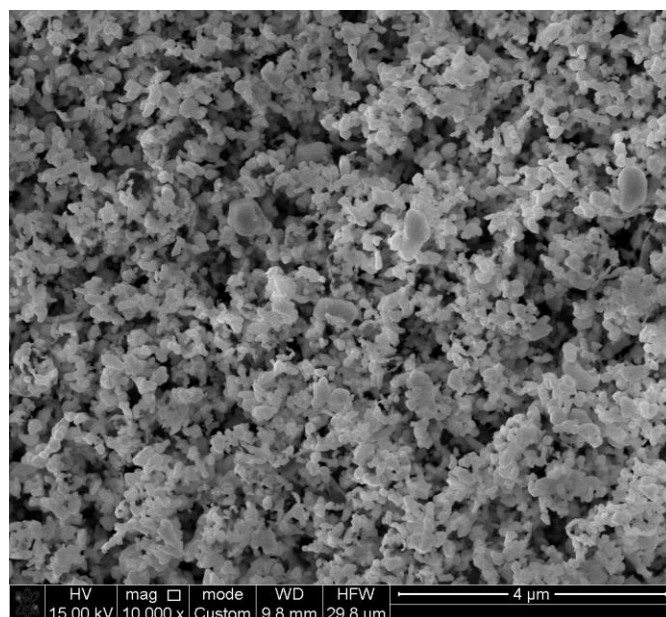
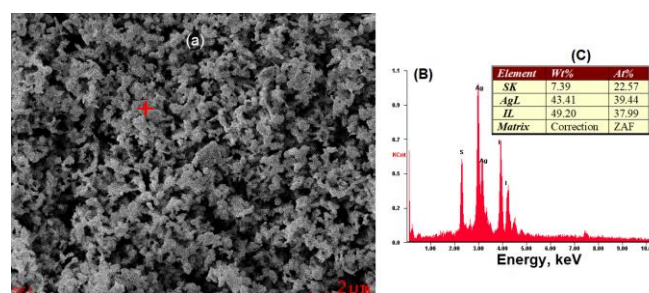**Figure 3** SEM image of AgI/S* with the addition of 1 ml of DMSO.

3.3. Nanocomposites S*/AgX in Pulverisette 5 mill

Above, we discussed the results of studying AgI/S* nanocomposites synthesized by reaction (2) in the 1-drum Pulverisette 6 mill with tungsten carbide milling tools. Below are the processed results of XRD (Figure 5) and Raman spectroscopy (Figure 6) of AgX/S* nanocomposites declared for completeness of the syntheses according to reactions (3) and/or Scheme 1c in the 4-drum Pulverisette 5 mill with stainless steel milling tools. XRD patterns of the S*/AgCl, S*/AgBr and S*/AgI synthesized in the DMSO medium (1–5 mL), pure sulfur (α–form) and corresponding cubic AgX phases are given in Figures 5 (a,b,c). It can be seen that they agree, complement and confirm the data in Figures S1, S3 for the presence of phases in S*/AgI and in Figures S4(a,b,c,d) for $D \sim 20$ nm and $\varepsilon \sim 0.2\%$. Discussing the data in Figures S5 (a,b), we have already noted that S*/AgI show a combination of S [42] and AgI [43] peaks with an unchanged position; their strong superposition takes place, and these effects are even more typical for S*/AgX nanocomposites obtained in the Pulverisette 5 mill, as shown in Figures 6 (a, b, c).

According to the analysis of samples S*/AgCl (Figures 6a), there are three Raman modes at 75, 86 and 240 cm^{-1} for pure AgCl. The peaks at 75 and 240 cm^{-1} wavenumbers are related to AgCl, while the peak at 86 cm^{-1} is characteristic of elemental Ag, which can be formed

under influence of the laser, because of the photosensitivity of AgCl and its decomposition [22]. Raman spectra for pure AgBr (Figures 6b) are represented by three characteristic peaks at about 70, 130 and 180 cm^{-1}. The peaks at 70 and 130 cm^{-1} can be attributed to Ag lattice vibrations. The peak at 180 cm^{-1} is conditioned by stretching of the Ag–Br bond, which is in agreement with the results for AgCl considering the difference in mass. For pure AgI (Figures 6c) two peaks at 74 and 109 cm^{-1} are seen. The four peaks at 89, 158, 223 and 477 cm^{-1} are attributed to sulfur, and, as compared to Figures S5, they shift to 83, 152, 219 and 474 cm^{-1}.

From Figures 5, 6 it can also be established that the amount of DMSO and the mill used have little effect on the results of XRD and Raman spectroscopy.

Figure 4 SEM image of the AgI/S* sample with the addition of 5 ml of DMSO: the studied field of EDAX application is given by a cross (a); the result of determining the elemental composition and it table form are given in (b) and in insertion (c).
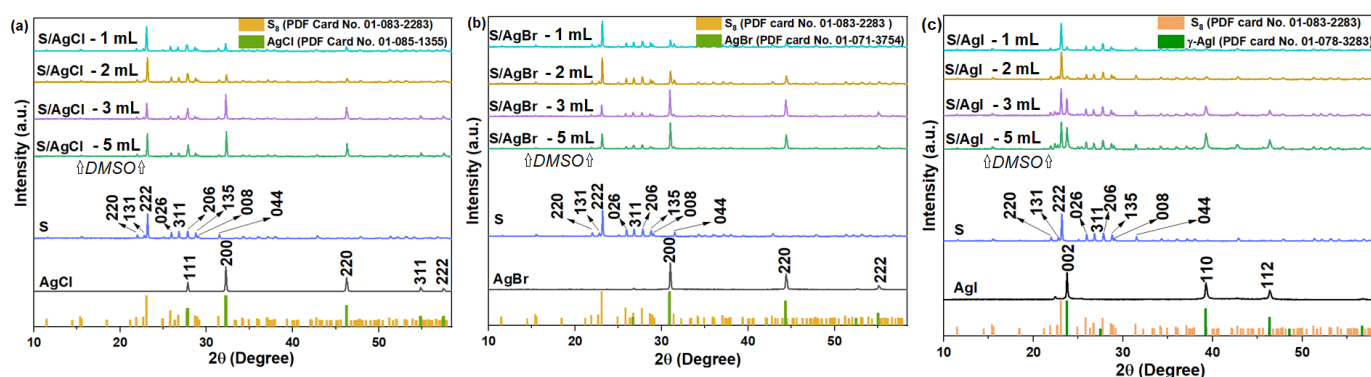
Figure 5 Results of XRD analysis of samples of mechanosynthesis of nanocomposites S*/AgX, X = Cl (**a**); Br (**b**); I (**c**) with the addition of 5, 3, 2 and 1 mL of DMSO in the Pulverisette 5 mill.
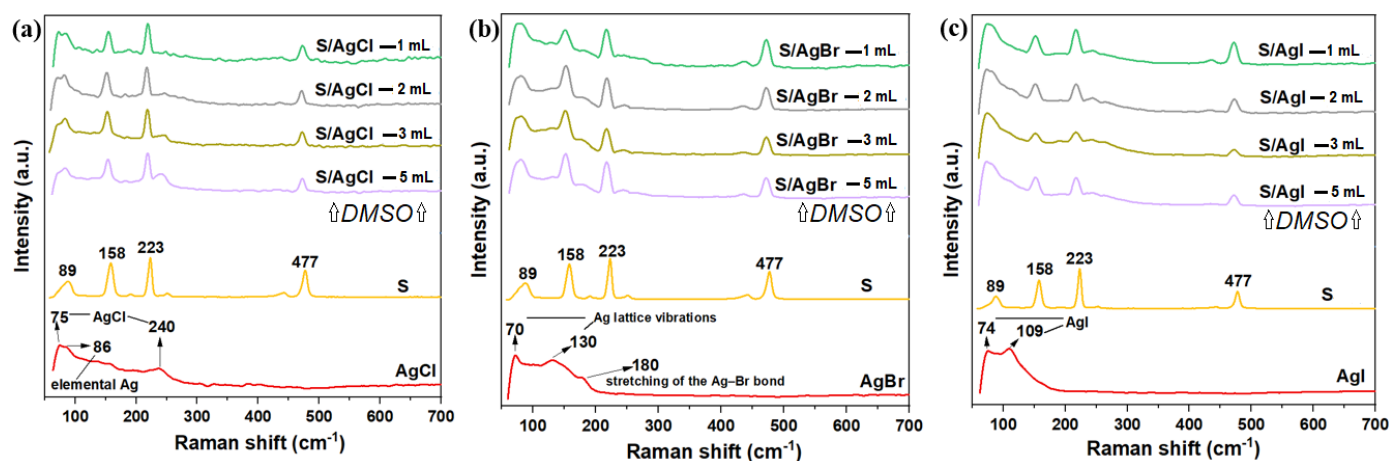
Figure 6 Raman spectra of samples of mechanosynthesis of nanocomposites S*/AgX, X = Cl (a); Br (b); I (c) with the addition of 5, 3, 2 and 1 ml of DMSO in the Pulverisette 5 mill.

DOI:

The proposed technical solution makes it possible to obtain, by single mechanical activation in a planetary ball mill with stainless steel fittings, sulfur-containing nanocomposites AgX/S* (X = Cl, Br, I) of powder precursors – $AgNO_3$, NH_4X, NH_4NO_3 (diluent [31]), commercial sulfur, and liquid phase – universal aprotic solvent dimethyl sulfoxide [19]. The predetermined content of nanosulfur in nanocomposites is provided by the process of dissolution-crystallization (recrystallization) of sulfur in dimethyl sulfoxide in the mechanochemical reactor [35].

4. Limitations

The most important problem for the proposed line of research is the correct assessment of the quantitative ratio of solid (powder precursors): liquid (solvent precursors). This is not the case, and, for example, in this work, for 10 grams of powder precursors, we took 1–5 ml of the liquid DMSO solvent. It is intuitively clear that more than 5 ml of DMSO seems unacceptable, but decreasing the amounts to less than 1 ml of DMSO seems to be the prospect for further work.

The second limitation is the choice of a solid-liquid system. In fact, there is no reason to believe that the sulfur-silver-halides-DMSO system considered here can claim exceptional scientific and applied significance. But the important thing is that there are many such systems, and there is always a chance of success.

The last issue concerns the choice of a mechanochemical reactor. In this study, we used, one might say, the highest-energy devices for mechanical activation – planetary ball mills. However, when working with semi-liquid (or semi-solid) systems, this is hardly necessary, and it seems that continuous mechanochemical reactors would be better suited here.

5. Conclusions

For the first time, the method of "mechanochemical recrystallization" in solid-phase systems with small additions of the liquid phase of the precursor solvent – dimethyl sulfoxide – was systematically studied and introduced into scientific practice. The essence of this method is demonstrated by the example of mechanical activation of 10 g of the $AgNO_3$–NH_4I–NH_4NO_3 (diluent)-S system with variable additions of DMSO (1–5 ml), which results in the mechanochemical synthesis of sulfur-containing AgI/S nanocomposites with a controlled content of nanosulfur. The specified content of nanosulfur in nanocomposites during their synthesis in mechanochemical reactors is taken equal to 50% by weight and is provided by the reaction process of dissolution-crystallization (recrystallization) of the initial sulfur and precursors in DMSO. The proposed method made it possible to obtain separately both nanosulfur and AgI/S nanocomposites by a single mechanical treatment of powdered precursors - AgNO3, NH4I, NH4NO3, technical sulfur and DMSO – in planetary ball mills Pulverisette 6 (single-drum; accessories – tungsten carbide) and Pulverisette 5 (four-drum; accessories – stainless steel). The method also includes ultrasonic washing of water-soluble components of mechanosynthesis with distilled water using a centrifuge and drying the obtained target product for 24 hours at a temperature of 70 °C.

● Supplementary materials

This manuscript contains supplementary materials, which are available on the corresponding online page.

● Author contributions

Conceptualization: F.K.U.
Data curation: M.M.B.
Formal Analysis: M.M.B., N.V.K., A.I.N.
Funding acquisition: F.K.U., N.N.K.
Investigation: F.K.U., N.N.K., A.I.N., D.N.Z.
Methodology: F.K.U., M.M.B., N.V.K.
Project administration: M.M.B., A.I.N.
Resources: M.M.B., A.I.N., D.N.Z.
Software: F.K.U., N.N.K.
Supervision: M.M.B., A.I.N.
Validation: M.M.B., N.V.K.
Visualization: F.K.U., M.M.B., N.N.K.
Writing – original draft: F.K.U., N.N.K.
Writing – review & editing: F.K.U.

● Conflict of interest

The authors declare no conflict of interest.

● Additional information

Author IDs:

Farit Kh. Urakaev, Scopus ID 35619573400;
Natalya V. Khan, Scopus ID 57214114418;
Almagul I. Niyazbayeva, Scopus ID 6505546558;
Dinar N. Zharlykasimova, Scopus ID 56912424400;
Mukhambetkali M. Burkitbayev, Scopus ID 8513885600.

Websites:

Sobolev Institute of Geology and Mineralogy, https://www.igm.nsc.ru/index.php/en;

Al-Farabi Kazakh National University, https://www.kaznu.kz/en.

References

1. Friščić T, Childs SL, Rizvi SAA, Jones W. The role of solvent in mechanochemical and sonochemical cocrystal formation: a solubility-based approach for predicting cocrystallisation outcome. CrystEngComm. 2009;11(3):418–426. doi:10.1039/B815174A

2. Meenatchi B, Renuga V. Protic ionic liquids assisted synthesis and characterization of sulfur nanoparticles and CdS and ZnS nanomaterials. Chem Sci Trans. 2015;4(2):577–587. doi:10.7598/cst2015.1028

3. Ying P, Yu J, Su W. Liquid-assisted grinding mechanochemistry in the synthesis of pharmaceuticals. Adv Synth Catal. 2021;363(5):1246-1271. doi:10.1002/adsc.202001245

4. Zaikin PA, Dyan OkT, Elanov IR, Borodkin GI. Ionic liquid-assisted grinding: An electrophilic fluorination benchmark. Molecules. 2021;26(19):5756. doi:10.3390/molecules26195756

5. Kosimov A, Yusibova G, Aruväli J, Paiste P, Käärik M, Leis J, Kikas A, Kisand V, Šmits K, Kongi N. Liquid-assisted grinding/compression: A facile mechanosynthetic route for the production of high-performing Co–N–C electrocatalyst materials. Green Chem. 2022;24(1):305–314. doi:10.1039/D1GC03433B

6. Loya JD, Li SJ, Unruh DK, Hutchins KM. Mechanochemistry as a tool for crystallizing inaccessible solids from viscous liquid components. Cryst. Growth Des. 2022;22(1):285–292. doi:10.1021/acs.cgd.1c00929

7. Baláž P, Achimovičová M, Baláž M, Billik P, Cherkezova-Zheleva Z, Criado JM, Delogu F, Dutková E, Gaffet E, Gotor FJ, Kumar R, Mitov I, Rojac T, Senna M, Streletskii A, Wieczorek-Ciurowa K. Hallmarks of mechanochemistry: from nanoparticles to technology. Chem Soc Rev. 2013;42(18):7571–7637. doi:10.1039/C3CS35468G

8. Boldyreva E. Mechanochemistry of inorganic and organic systems: what is similar, what is different? Chem Soc Rev. 2013;42(18):7719–7738. doi:10.1039/C3CS60052A

9. Michalchuk AA, Boldyreva EV, Belenguer AM, Emmerling F, Boldyrev VV. Tribochemistry, mechanical alloying, mechanochemistry: what is in a name? Front. Chem. 2021;9(1):685789. doi:10.3389/fchem.2021.685789

10. Boldyreva EV. Spiers Memorial Lecture: Mechanochemistry, tribochemistry, mechanical alloying – retrospect, achievements and challenges. Faraday Discuss. 2023;241:9–62. doi:10.1039/D2FD00149G

11. Matsuoka M, Danzuka K. Solid-state recrystallization behavior of binary inorganic salt systems by mechanochemical processing. J Chem Eng Japan. 2009;42(6):393–399. doi:10.1252/jcej.09we068

12. Katsenis A, Puškarić A, Štrukil V, Mottillo C, Julien PA, Užarević K, Pham M-H, Do T-O, Kimber SAJ, Lazić P, Magdysyuk O, Dinnebier RE, Halasz I, Friščić T. In situ X-ray diffraction monitoring of a mechanochemical reaction reveals a unique topology metal-organic framework. Nat Commun. 2015;6:6662. doi:10.1038/ncomms7662

13. Urakaev FKh, Khan NV, Shalabaev ZhS, Tatykaev BB, Nadirov RK, Burkitbaev MM. Synthesis and photocatalytic properties of silver chloride/silver composite colloidal particles. Colloid J. 2020;82(1):76–80. doi:10.1134/S1061933X20010160

14. Nieto-Castro D, Garcés-Pineda FA, Moneo-Corcuera A, Pato-Doldan B, Gispert-Guirado F, Benet-Buchholz J, Galán-Mascarós JR. Effect of mechanochemical recrystallization on the thermal hysteresis of 1D Fe^{II}-triazole spin crossover polymers. Inorg Chem. 2020;59(12):7953–7959. doi:10.1021/acs.inorgchem.9b03284

15. Kadja GTM, Suprianti TR, Ilmi MM, Khalil M, Mukti RR, Subagjo. Sequential mechanochemical and recrystallization methods for synthesizing hierarchically porous ZSM-5 zeolites. Microporous Mesoporous Mater. 2020;308:110550. doi:10.1016/j.micromeso.2020.110550

16. Zyryanov VV, Petrov SA, Ulihin AS. Mechanically activated synthesis, characterization and conducting properties of complex perovskites for Ag-based metal-matrix nanocomposites. Ceram Int. 2021;47(20):29499–29503. doi:10.1016/j.ceramint.2021.07.118

17. Zyryanov VV. Mechanically assisted chemical interaction of doped bismuth oxide with silver. Solid State Ionics. 2022;383:115987. doi:10.1016/j.ssi.2022.115987

18. Dubadi R, Huang SD, Jaroniec M. Mechanochemical synthesis of nanoparticles for potential antimicrobial applications. Mater. 2023;16(4):1460. doi:10.3390/ma16041460

19. Burkitbayev MM, Urakaev FKh. Temperature dependence of sulfur solubility in dimethyl sulfoxide and changes in concentration of supersaturated sulfur solutions at 25 degrees C. J Mol Liq. 2020;316:113886. doi:10.1016/j.molliq.2020.113886

20. Du G-X, Xue Q, Ding H, Li Z. Mechanochemical effects of ZnO powder in a wet super-fine grinding system as indicated by instrumental characterization. Int J Min Process. 2015;141:15–19. doi:10.1016/j.minpro.2015.06.008

21. Lu J, Lu Z, Li X, Xu H, Li X. Recycling of shell wastes into nanosized calcium carbonate powders with different phase compositions. J Clean Prod. 2015;92:223–229. doi:10.1016/j.jclepro.2014.12.093

22. Lu J, Cong X, Li Y, Hao Y, Wang C. Scalable recycling of oyster shells into high purity calcite powders by the mechanochemical and hydrothermal treatments. J Clean Prod. 2018;172:1978–1985. doi:10.1016/j.jclepro.2017.11.228

23. Kurniawan T, Muraza O, Hakeem AS, Al-Amer AM. Mechanochemical route and recrystallization strategy to fabricate mordenite nanoparticles from natural zeolites. Cryst Growth Des. 2017;17(6):3313–3320. doi:10.1021/acs.cgd.7b00295

24. de Oliveira Y.S., Oliveira A.C., Ayala A.P. Mechanochemically induced solid state transformations: The case of raloxifene hydrochloride. Eur J Pharm Sci. 2018;114:146–154. doi:10.1016/j.ejps.2017.11.028

25. Yang P, Li X, Li Z, Fang X, Zhang K, Zhuang W, Wu J, Zhu C, Ying H. Green mechanochemical strategy for the construction of a new bio-based nylon 5_24T ternary salt. ACS Sustain Chem Eng. 2022;10(11):3513–3520. doi:10.1021/acssuschemeng.1c07869

26. Urakaev FKh, Bulavchenko AI, Uralbekov BM, Massalimov IA, Tatykaev BB, Bolatov AK, Zharlykasimova DN, Burkitbayev MM. Mechanochemical synthesis of colloidal sulphur particles in the $Na_2S_2O_3$–$H_2(C_4H_4O_4)$–Na_2SO_3 system. Colloid J. 2016;78(2):210–219. doi:10.1134/S1061933X16020150

27. Shalabayev Zh, Baláž M, Daneu N, Dutkova E, Bujňáková Z, Kaňuchová M, Dankova Z, Balážová Ľ, Tkáčiková Ľ, Urakaev F, Burkitbayev M. Sulfur-mediated mechanochemical synthesis of spherical and needle-like copper sulfide nanocrystals with antibacterial activity. ACS Sustain Chem Eng. 2019;7(15):12897–12909. doi:10.1021/acssuschemeng.9b01849

28. Shalabaev ZS, Urakaev FK, Baláž M, Khan NV, Burkitbaev MM. Method for obtaining needle-like copper sulfide (II) nanocrystals. Patent of the Republic of Kazakhstan for utility model No. 5287. Bulletin number: 32. Bulletin date: 14.08.2020. https://gosreestr.kazpatent.kz/Utili-tymodel/DownLoadFilePdf?patentId=326616&lang=ru

29. Khan N, Baláž M, Burkitbayev M, Tatykayev B, Shalabayev Z, Nemakayeva R, Jumagaziyeva A, Niyazbayeva A, Rakhimbek I, Beldeubayev A, Urakaev F. DMSO- mediated solvothermal synthesis of S/AgX (X = Cl, Br) microstructures and study of their photocatalytic and biological activity. Appl Surf Sci. 2022;601:154122. doi:10.1016/j.apsusc.2022.154122

30. Khan NV, Baláž M, Burkitbayev MM, Tatykayev BB, Shalabayev ZhS., Niyazbayeva AI, Urakaev FKh. Solvothermal DMSO-mediated synthesis of the S/AgI microstructures and their testing as photocatalysts and biological agents. Int J Biol Chem. 2022;15(1):79–89. doi:10.26577/ijbch.2022.v15.i1.09

31. Urakaev FKh. Mechanochemical synthesis of nanoparticles by a dilution method: determination of the particle mixing coefficient in a ball mill. Mendeleev Commun. 2012;22(4):215–217. doi:10.1016/j.mencom.2012.06.016

32. Urakaev FK, Burkitbaev MM, Uralbekov BM, Shalabaev ZS. Method for producing sulfur nanoparticles from solutions in dimethyl sulphoxide, using solution of sulfur in dimethyl sulfoxide saturated at room temperature with specific sulfur concentration when diluted with water or acetone. Patent EA33075-B1. Publ. 30 Aug 2019. Derwent 2019-85527S.

33. Urakaev FKh, Burkitbayev MM, Khan NV. Biological activity of sulfur nanoparticles in the sulfur–dimethyl sulfoxide–water system. Int J Biol Chem. 2022;15(2):54–75. doi:10.26577/ijbch.2022.v15.i2.09

34. Burkitbaev MM, Khan NV, Madikasimova MS, Oskenbai AK, Urakaev FKh. Method for obtaining sulfur-containing nanocomposites. Patent of the Republic of Kazakhstan for utility model No. 5241. Bulletin number: 30. Bulletin date: 30.07.2020. https://gosreestr.kazpatent.kz/Utilitymodel/DownLoadFilePdf?patentId=325175&lang=ru

35. Urakaev FKh. Preparation of $NaIn(WO_4)(2)$ nanocrystals and a charge for crystal growth via the free-of-rubbing mechanical activation of the Na_2CO_3–In_2O_3–WO_3 system. Mendeleev Commun. 2016;26(6):546–548. doi:10.1016/j.mencom.2016.11.030

36. LeBel RG, Goring DAI. Density, viscosity, refractive index, and hygroscopicity of mixtures of water and dimethyl sulfoxide. J Chem Eng Data. 1962;7(1):100–101. doi:10.1021/je60012a032

37. Ellson R, Stearns R, Mutz M, C Brown C, Browning B, Harris D, Qureshi S, Shieh J, Wold D. In situ DMSO hydration measurements of HTS compound libraries. Comb Chem High Throughput Screen. 2005;8(6):489–498. doi:10.2174/1386207054867382

38. Waybright TJ, Britt JR, McCloud TG. Overcoming problems of compound storage in DMSO: solvent and process alternatives. J Biomol Screen. 2009;14(6):708–715. doi:10.1177/1087057109335670

39. Rabiei M, Palevicius A, Dashti A, Nasiri S, Monshi A, Doustmohammadi A, Vilkauskas A, Janusas G. X-ray diffraction analysis and Williamson-Hall method in USDM model for estimating more accurate values of Stress-Strain of unit cell and super cells ($2 \times 2 \times 2$) of hydroxyapatite, confirmed by Ultrasonic Pulse-Echo Test. Mater (Basel). 2021;14(11):2949. doi:10.3390/ma14112949

40. Himabindu B, Latha Devi NSMP, Rajini Kanth B. Microstructural parameters from X-ray peak profile analysis by Williamson-Hall models; A review. Mater Today Proceed. 2021;47(14):4891–4896. doi:10.1016/j.matpr.2021.06.256

41. Tirpude MP, Tayade NT. Frustrate microstructures composed PbS cluster's size perspective from XRD by variant models of Williamson-Hall plot method. Preprint. 2022;25:36. doi:10.21203/rs.3.rs-1586320/v1

42. Nims C, Cron B, Wetherington M, Macalady J, Cosmidis J. Low frequency Raman spectroscopy for micron-scale and in vivo characterization of elemental sulfur in microbial samples. Sci Rep-UK. 2019;9(1):7971. doi:10.1038/s41598-019-44353-6

43. Assis M, Groppo Filho FC., Pimentel DS., Robeldo T, Gouveia AF, Castro TFD, Fukushima HCS, de Foggi CC, da Costa JPC, Borra RC, Andrés J, Longo E. Ag nanoparticles / AgX (X= Cl, Br, I) composites with enhanced photocatalytic activity and low toxicological effects. Chem Sel. 2020;5(15):4655–4673. doi:10.1002/slct.202000502